In vivo dynamics of retinal injury and repair in the *rhodopsin* mutant dog model of human retinitis pigmentosa

Artur V. Cideciyan*†, Samuel G. Jacobson*, Tomas S. Aleman*, Danian Gu‡, Susan E. Pearce-Kelling§, Alexander Sumaroka*, Gregory M. Acland§, and Gustavo D. Aguirre‡

*Department of Ophthalmology and ‡Section of Medical Genetics, University of Pennsylvania, Philadelphia, PA 19104; and §James A. Baker Institute for Animal Health, Cornell University, Ithaca, NY 14853

Edited by Jeremy Nathans, The Johns Hopkins University School of Medicine, Baltimore, MD, and approved February 22, 2005 (received for review December 2, 2004)

Genetic and environmental factors modify the severity of human neurodegenerations. Retinal degenerations caused by *rhodopsin* gene mutations show severity differences within and between families and even within regions of the same eye. Environmental light is thought to contribute to this variation. In the naturally occurring dog model of the human disorder, we found that modest light levels, as used in routine clinical practice, dramatically accelerated the neurodegeneration. Dynamics of acute retinal injury (consisting of abnormal intraretinal light scattering) were visualized *in vivo* in real time with high-resolution optical imaging. Long term consequences included fast or slow retinal degeneration or repair of injury depending on the dose of light exposure. These experiments provide a platform to study mechanisms of neuronal injury, repair, compensation, and degeneration. The data also argue for a gene-specific clinical trial of light reduction in human *rhodopsin* disease.

apoptosis | *in vivo* imaging | light damage | retinal degeneration

Fundamental insight into neuronal dysfunction and death in slowly progressive neurodegenerative disorders has come from elucidation of causative mutant genes and the compromised molecular pathways in hereditary forms of these complex diseases (1). Adding to the effects of gene abnormalities are environmental factors. The interplay of gene and environment may help explain clinical variability in onset and progression within genotypes, and detailed knowledge of the interaction may permit testing of hypotheses with therapeutic implications.

The slowly progressive inherited retinal degenerations, known as retinitis pigmentosa (RP), have undergone a revolution in understanding of molecular causation, with >100 cloned genes and a wealth of animal models to study pathogenesis of retinal cell death (2). As an accessible part of the brain, the retina and thus retinal dystrophies are well-suited for study of gene–environment interactions. Light is an environmental insult that can be quantitatively delivered to the retina, and it has been investigated for decades as a retinotoxin (3–5).

Rhodopsin (RHO) encodes the light-sensing G protein-coupled receptor in the membranes of rod photoreceptors, the neurons specialized for night vision. *RHO* mutations were the first genetic cause discovered for human RP (6) and are now predicted to be the most common cause of RP (7). Transgenic rodents with *RHO* mutations have been used to seek mechanisms of retinal degeneration and also to explore the effects of environmental light on disease severity (8, 9). The consensus is that light can be an accelerator of these retinal degenerations, lending support to inferences from human case reports (10).

We recently identified a naturally occurring canine model of autosomal dominant RP caused by *RHO* mutation and demonstrated that the phenotype strongly resembled that in humans (11, 12). Exploiting the close similarity in eye size and preretinal light transmission characteristics between dog and man, we tested the hypothesis that environmental light may be a potential accelerator of the natural history of visual loss in this large-animal model. First, we asked a question of immediate clinical relevance: Is there any effect on the retina of the light exposure from routine clinical testing, specifically retinal photography, the time-honored method for monitoring human retinal diseases including RP (13, 14). To our surprise, clinical photography caused retinal degeneration in the exact montage pattern on the retina as the circular light flashes. This result prompted further studies using *in vivo* high-resolution imaging methods to study focal light exposures well below the normal phototoxicity threshold and their effect on the *RHO* mutant dog retina. In addition to evidence of retinal damage from light, we provide evidence in a genetic retinal degeneration of repair at lower doses of light. The natural history of retinal degeneration in human *RHO* mutations may result from a complex interaction with environmental light that includes continuous attempt at repair, cellular compensation, and increased risk of cell death (1, 15).

Methods

Animals. Dogs heterozygous for the T4R mutation in the *RHO* gene ($n = 11$, ages 3–6 mos) and wild-type controls ($n = 5$, ages 3–7 mos) were dark adapted and had pupils dilated (11). Experiments were in accordance with the Association for Research in Vision and Ophthalmology Resolution and institutional review boards.

Light Exposure. Small regions of the retina (Fig. 6, which is published as supporting information on the PNAS web site) were exposed to a 60-s duration of visible light. For each eye, a region in the tapetal retina ≈8 mm superior to the optic nerve was exposed first, and 10 min later a region in nontapetal retina ≈5 mm inferior to optic nerve was exposed. Light source radiance was measured (IL1700, International Light, Newburyport, MA), and retinal irradiances were estimated. Two exposure intensities estimated to achieve lower (0.1 mW·cm^{-2}) and higher (1 mW·cm^{-2}) retinal irradiances were used; the doses were 6 and 60 mJ·cm^{-2}, respectively. The lower dose was 1,500- to 6,000-fold less than retinal damage thresholds for white or medium-wavelength light in different species (16–18). In another experiment, dogs underwent "stereo" fundus photography by an experienced fundus photographer using a conventional camera (FF4, ZeissMeditec, Dublin, CA) at settings typically used in a human eye clinic (flash intensity, 60 Ws; observation/focusing, 2). Seven standard overlapping 30° fields were photographed (two flashes per field). Estimated total dose at each retinal region was 50

This paper was submitted directly (Track II) to the PNAS office.

Abbreviations: OCT, optical coherence tomography; *RHO*, *rhodopsin*; RP, retinitis pigmentosa; LRP, longitudinal reflectivity profile; IS, inner segment; OS, outer segment; RPE, retinal pigment epithelium; ERG, electroretinogram; AP-1, activator protein 1; OPL, outer plexiform layer; ONL, outer nuclear layer.

†To whom correspondence should be addressed at: Scheie Eye Institute, 51 North 39th Street, Philadelphia, PA 19104. E-mail: cideciya@mail.med.upenn.edu.

mJ·cm^{-2}. In a third experiment, a standard (International Society for Clinical Electrophysiology of Vision) electroretinogram (ERG) protocol of four light flashes was performed with full-field stimuli, estimated to result in a retinal dose of 0.002 mJ·cm^{-2}.

***En Face* Imaging.** A confocal scanning laser ophthalmoscope (HRA, Dossenheim, Germany) was used to document the e*n face* appearance of the dog fundus with infrared (840 nm) illumination. Overlapping retinal regions were sequentially imaged, and wide-field composite images were formed with custom software. Images of the same retinal region acquired at different times were registered by using blood vessel crossings as landmarks.

Optical Coherence Tomography (OCT). Longitudinal (cross-sectional) reflectivity (backscatter) profiles (LRP) through different retinal layers were obtained with OCT (ZeissMeditec; ref.19) at 840 nm by using our published methods (11, 20–22). OCTs were performed in groups of parallel linear ("raster") scans (6 mm in length, separated by 0.15, 0.3, or 0.6 mm) in retinal regions before and after focal light exposure. Multiple overlapping groups of scans covered the retinal region of interest. Video fundus images with deep red illumination were acquired for each scanned segment.

Postacquisition processing of data was performed with custom programs. Precise location and orientation of each scan relative to fundus features were determined. LRPs constituting each OCT scan were allotted to 0.3 × 0.3 mm^2 bins in a rectangular coordinate system centered at the optic nerve; resulting LRPs in each bin were aligned by using a dynamic cross-correlation algorithm (20, 21) and averaged. Maps of the same retinal region acquired at different times were registered with respect to each other by using retinal features coregistered to each map. Retinal thickness was defined to be the distance between previously defined features T1 (vitreo-retinal interface) and T4 (maximal slope vitread to the signal maximum) on averaged LRPs (11, 20–22). Missing data were interpolated bilinearly, thickness values were mapped to a pseudo-color scale, and locations of blood vessels and optic nerve head were overlaid for reference.

The change in intensity of the light backscattered from different retinal lamina was quantified as a function of time after light exposure by using two types of reference values: at the same retinal location preexposure or at a neighboring nonexposed retinal location. The change in backscatter intensity, B, as a function of depth, d, was specified as $B(d) = 10^{[0.00135\times(C(d)-C_0(d))]}$, where $C(d)$ and $C_0(d)$ are counts reported by the OCT instrument at the postexposure time and reference, respectively. Assuming no major changes in absorption and anisotropy coefficients of retinal tissue, $B(d)$ would be proportional to the ratio of the intensities of light backscattered for the two conditions.

Histopathology and Immunocytochemistry. Retinal sections for morphology were prepared as described (11). Orientation of the eyes was based on fundus diagrams made at the time of light exposure and *en face* infrared images. One-micrometer or 10-μm sections were taken beginning outside the borders of the lesion and progressing to its center. For immunocytochemical studies, sections were labeled with rabbit anti mouse RPE65 polyclonal antibody (PETLET), mouse monoclonal antibody K16-107C directed at the C-terminal domain of opsin (23), and nuclei labeled with DAPI.

Activator Protein 1 (AP-1) DNA-Binding Activity. One eye of dogs had indirect ophthalmoscopy, and a series of overlapping retinal photographs were taken with a hand-held fundus camera. After light exposure, dogs were dark-adapted, and retinas were harvested 1 or 6 h later. EMSA analysis was used to determine AP-1 activation. Nuclear protein extracts were prepared with a differential centrifugation procedure after homogenization (24) and hybridized with the AP-1 consensus oligonucleotide GGC TTG ATG AGT CAG CCG GAA (Promega) labeled with [γ-^{32}P]ATP. The products were analyzed with 2–20% gradient polyacrylamide gels in a TBE system (90 mM Tris/64.6 mM boric acid/2.5 mM EDTA, pH 8.3), and the AP-1 complex was detected as the shifted band. The DNA-binding activity of AP-1 was identified based on the intensity of the shifted bands quantified by fluorography.

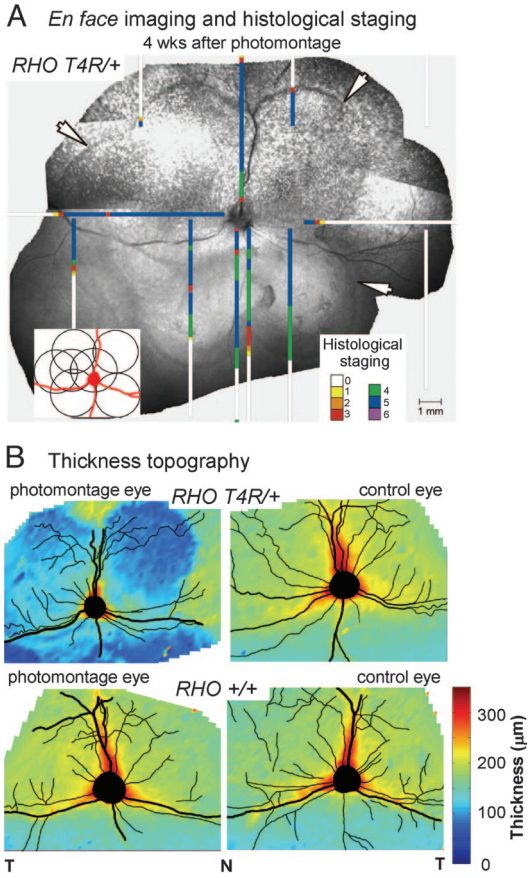

Fig. 1. Consequences of clinical human retinal photography in the *RHO* mutant dog. (*A*) Digital montage of *en face* infrared images 4 wk after photography using seven standard overlapping fields (*Inset*). Superimposed on the retinal photograph are maps of retinal disease staging by light microscopy in this dog. Higher numbers represent more severe disease (11). (*B*) Topographical maps of retinal thickness on a pseudocolor scale derived from cross-sectional images. T, temporal; N, nasal.

Results

Retinal Degeneration 1 Month After Clinical Retinal Photography in the *RHO* Mutant Dog. The clinical examination for diagnosis and monitoring of many human retinal diseases commonly includes retinal photography and ERG. We evaluated the effect of the modest light exposures associated with standard versions of these two procedures in *RHO* mutant and wild-type dogs. A photographic montage (Fig. 1*A Inset*) was performed in right eyes, whereas left eyes served as unphotographed controls. Four weeks later, *en face* infrared imaging of the photographed eye of the *RHO* mutant dog showed lesions that were lighter than surrounding retina but with darker scalloped edges following the outer boundaries of the overlapping photographed fields (Fig. 1*A*, arrows). Control eyes and the photographed eye of the wild-type dog had no abnormalities. Topographical maps of retinal thickness by cross-sectional imaging (Fig. 1*B*) indicated dramatic thinning only in photographed regions of the *RHO* mutant dog eye but normal thickness in the photographed eye of a wild-type dog and in unphotographed control eyes. ERGs were performed with a similar experimental design as for photography. *En face* infrared imaging and maps of

retinal thickness in the eyes that had ERGs did not show differences from control eyes (data not shown).

Histology in the photographed eye of the *RHO* mutant dog showed extensive retinal degeneration limited to the exposed areas (Fig. 1*A*). The photoreceptor layer was either absent or reduced to a single row of nuclei. There was RPE cell loss, but inner retinal structure was preserved. The unphotographed fellow eye showed normal retinal structure; similarly, there were no histological abnormalities associated with the ERG procedure.

Increased Intraretinal Backscatter Within 1 h After Focal Light Exposure. Spatial and temporal properties of the retinal injury caused by light in *RHO* mutant dogs were further explored by using a small circular light exposure with an estimated retinal irradiance dose (60 mJ·cm^{-2}) equivalent to retinal photography. Two retinal locations, one superior (tapetal) and the other inferior (nontapetal), were exposed to light and then monitored with noninvasive imaging for several hours and at 24 h. By *en face* imaging, the two sites of light exposure showed no apparent changes at 10 min, but, by 2 h, circular lesions were apparent (Fig. 2*A*). The superior lesion in tapetal retina appeared darker than surrounding nonexposed retina, and the inferior lesion appeared lighter against the background of darkly pigmented nontapetal fundus. By 24 h, both lesions became more distinctly demarcated from surrounding retina.

Cross-sectional images at 1 h after light exposure were markedly different from images taken preexposure (Fig. 2*B*). In the exposed regions, there was increased reflectivity originating from structures deep in the retina (Fig. 2*B*, thin arrows). There was also a shift of the deep high reflectivity toward the retinal surface (Fig. 2*B*, thick arrows), giving the appearance of overall retinal thinning. To probe the details of intraretinal changes within the first 24 h after light exposure, we used the LRPs that constitute the cross-sectional images. LRP waveform features have been shown to relate to the retinal laminae traditionally defined by light microscopy (20–22). Histological sections from superior (Fig. 2*C*) and inferior (Fig. 2*F*) sites are shown from the unexposed eye of a *RHO* mutant dog for comparison with LRPs from these locations in mutant dogs (before light exposure) overlaid on LRPs from wild-type dogs (Fig. 2 *D* and *G*; Control). Near the vitreo-retinal interface (retinal depth = 0 μm), there is a peak of reflectivity, and progressively deeper in the retina there are high and low reflectivities representing plexiform and nuclear layers, respectively. In the superior retina, the highest peak of reflectivity deep in the retina of control eyes is formed by photoreceptor inner segments (IS) and outer segments (OS), RPE, choriocapillaris, and tapetum. In the inferior retina, peak reflection includes photoreceptor IS/OS, RPE, and choriocapillaris.

Within 30 min after light exposure, superior retinal locations showed abnormally increased intraretinal backscatter (Fig. 2*D*, red) encompassing tissues starting at ≈80 μm from the vitreo-retinal interface [corresponding to the outer plexiform layer (OPL)], and continuing to ≈190 μm in retinal depth (corresponding to IS/OS and RPE). Between 1 and 1.5 h after exposure, there was increased abnormal backscatter, especially near the IS/OS, such that the locus of peak backscatter within the retina had moved ≈25 μm closer to the vitreous. At 3.5 h and later time points, the deeper component of the abnormal backscatter was not observable; the peak reflection was near control depth but showed reduced size. By 24 h, there was an increase in intraretinal backscatter and involvement of the inner retina (corresponding to tissues vitreal to OPL). Peak reflection was reduced in size and moved in the scleral direction, giving the impression of a thickened retina. Assuming no major changes in absorption and anisotropy coefficients of retinal tissue, scatter coefficients would be expected to increase 13-fold near IS/OS at 1 h and 7-fold near the outer nuclear layer (ONL) at 24 h (Fig. 2*E*). Light exposure in the inferior retina led to similar changes in intraretinal backscatter except they were slower to develop (e.g., no abnormality detected at 30 min after exposure, Fig. 2*G*) and inner retinal abnormalities were less apparent (Fig. 2 *F–H*). *En face* images also showed lesions less visible and of smaller extent in inferior retina compared with superior retina (Fig. 2*A*).

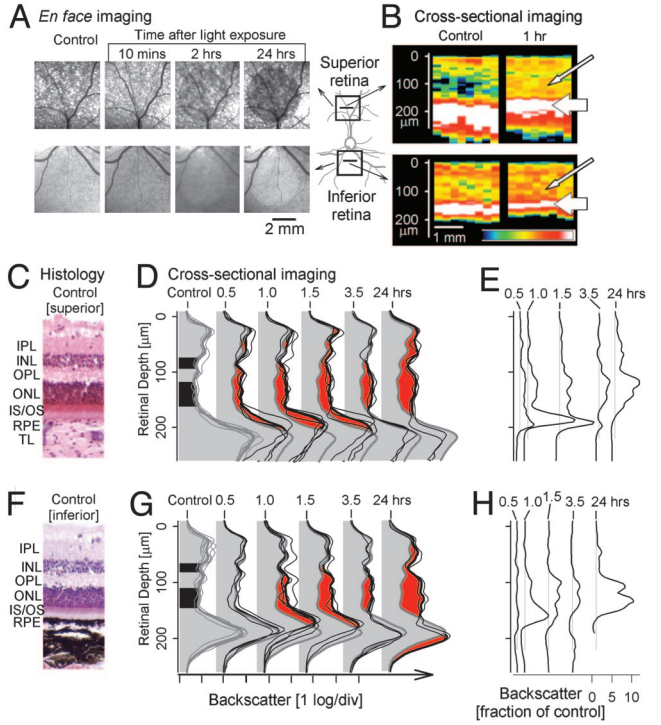

Fig. 2. *In vivo* detection of retinal alterations shortly after light exposure. (*A*) *En face* images in superior (*Upper*) and inferior (*Lower*) retinal locations before and after focal light exposure in a *RHO* mutant dog. (*B*) Cross-sectional images of infrared light backscatter intensity mapped to a pseudocolor scale in superior and inferior retina before and 1 h after the exposure. Vitreous is above each tomogram. Thin arrows point to regions of increased intraretinal light scatter after exposure; thick arrows point to the apparent vitreal movement of peak reflection. (*C* and *F*) Control retinal morphology from an unexposed eye of a *RHO* mutant dog at the superior and inferior locations of the focal light exposures. IPL, inner plexiform layer; INL, inner nuclear layer; TL, tapetum lucidum. (*D* and *G*) LRPs near the center of focal light exposures before and after exposure. Each thin trace represents data from a different eye. Thick gray traces are the average of control LRPs, and thick black traces are the average of LRPs at the specified time after exposure. Control traces include three unexposed *RHO* mutant eyes and one exposed and one unexposed wild-type eye. Black fill on the control LRPs delimits the two troughs of low backscatter corresponding to ONL and INL. Red fill represents the increase in intraretinal scatter as compared with control at each time point after the exposure. (*E* and *H*) Estimated change in the scatter coefficient of the retinal tissue as a function of retinal depth and time after the focal light exposure in superior and inferior loci. Curves have been shifted for clarity; gray vertical lines demarcate no change from control (unity ratio) for each time point.

Early Morphological Abnormalities and Induction of AP-1 After Light Exposure. Histopathology performed 2 h after the (60 mJ·cm^{-2}) light exposure showed massive shedding of OS tips; these OS were located in the interphotoreceptor space or engulfed by RPE cells. OS were short, disorganized, and fragmented (Fig. 3 *C* and *D*). There was increased spacing between photoreceptor (ONL) nuclei; some ONL nuclei were pyknotic. Opsin labeling and distribution in the OS was normal, although the shortening and fragmentation were apparent in most fields (Fig. 3*D*). At 24 h after exposure, OS were fragmented, and IS and OS were markedly shortened. There were pyknosis and edema of ONL (Fig. 3 *E* and *F*). In some fields, membranous whorls accumulated in the interphotoreceptor space adjacent to the apical RPE (Fig. 3*F*). In the exposed areas, many RPE cells were slightly swollen, and the distribution of their cytoplasmic organelles was altered. The transition between the

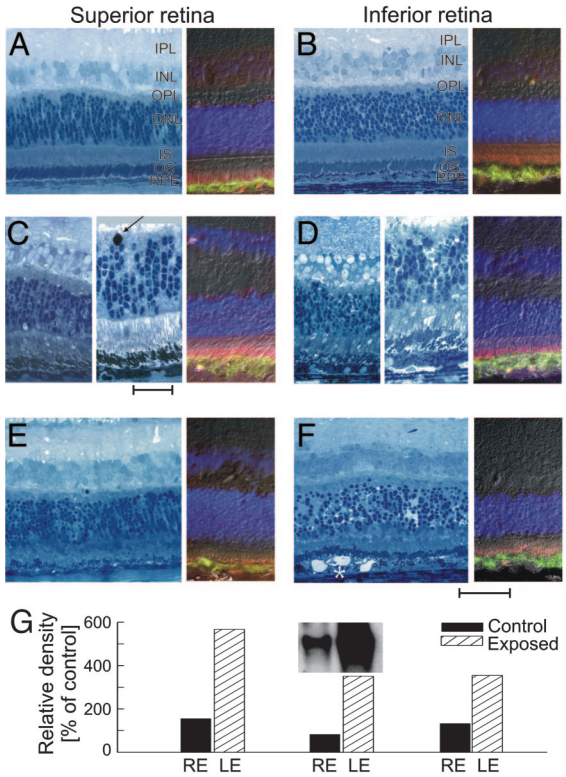

Fig. 3. Histopathology, immunocytochemistry, and AP-1 induction studies at early times after light exposure. (*A* and *B*) Control retina peripheral to the focal exposure. (*C* and *D*) Near center of lesion 2 h after exposure, there is massive shedding of rod photoreceptor OS tips that are located in the interphotoreceptor space or engulfed by RPE. OS are shorter, disorganized, and fragmented. Shown is the large pyknotic nucleus at the ONL/OPL interface (arrow). (*E* and *F*) Near center of lesion 24 h after exposure showing pyknosis of ONL, perinuclear and internuclear swelling in ONL, marked loss of rod and cone OS, and shortening of IS. RPE shows altered intracellular organization, and membranous whorls (*) accumulate in the interphotoreceptor space. (Scale bar is 50 μm for most panels, except *Center* of *C* and *D*, where scale bar is 25 μm.) Immunocytochemistry (*A–F Right*) used RPE65 (green) and opsin (red) antibodies to label the RPE and photoreceptor OS, respectively; DAPI labels the nuclei in all retinal layers. (*G*) Increase in AP-1 activation in three *RHO* mutant dogs 1 h after light exposure.

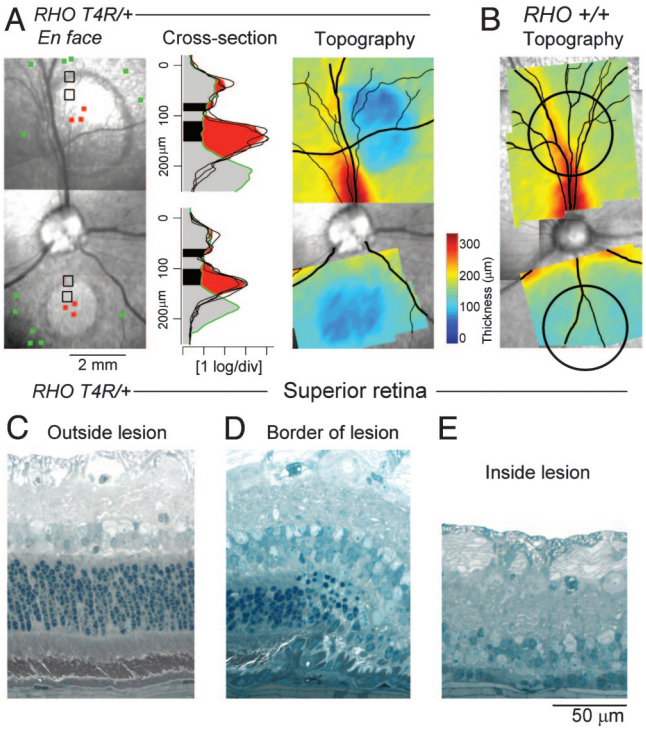

Fig. 4. Late retinal alterations after light exposure. (*A*) *En face* infrared images of a *RHO* mutant dog 4 wk after light exposure in superior and inferior retinal regions. Cross-sectional images near the center of the lesion (red squares) compared with loci outside the exposed region (green squares) demonstrate loss of the photoreceptor layer. Topographical maps show the retinal thickness on a pseudocolor scale and are superimposed on the *en face* image. (*B*) Topographical thickness maps in a wild-type dog 4 wk after focal exposures (black circles) indicate no change. (*C–E*) Histological changes 4 wk after focal exposure in the same *RHO* mutant dog as shown in *A* in the superior retina. Regions shown are outside, inside, and at the border between light-exposed and nonexposed regions. (*C*) Outside the lesion, the retina is normal, but there are abrupt changes at the border, with loss of outer retinal tissue (*D*). Inside the light-exposed area (*E*), photoreceptors and RPE are not present.

light-exposed and nonexposed regions was abrupt. Outside the zone of light exposure, retinal structure and immunolabeling with anti-opsin and RPE65 antibodies was normal (Fig. 3 *A* and *B*).

We also examined the association of AP-1 activation and light exposure in the *RHO* mutant dog retina for comparison with recent light damage literature (5). Within 1 h of the light exposure, EMSA detected an ≈4-fold increase (n = 3; range, 3.5–5.7) in AP-1 activation (Fig. 3*G*), implicating involvement of this transcription factor soon after the light stress. The nonexposed eye had AP-1 levels comparable with those in dark-adapted normal or *RHO* mutant dogs. AP-1 level was similarly elevated 6 h after light exposure in a *RHO* mutant retina.

Severe Outer Retinal Degeneration 1 Month After Focal Light Exposure. After 4 wk, two circular sites of light exposures had formed distinct lesions on *en face* infrared imaging in a *RHO* mutant dog (Fig. 4*A Left*). Cross-sectional images sampled near the center of the lesions allowed determination of intraretinal light scatter distribution (Fig. 4*A Center*). The vitreo-retinal interface and adjacent inner retinal reflectivities were similar to those of wild-type dog retina. There was a single deep trough of reflectivity, likely corresponding to the inner nuclear layer. Deeper retinal laminae, however, were not discernible, and the highest peak reflection was now closer by ≈100 μm to the retinal surface, a pattern suggesting severe outer retinal tissue loss (20–22). Topography of retinal thickness was also performed with cross-sectional imaging and showed dramatic retinal thinning at the locations of the two light exposures in the *RHO* mutant dog (Fig. 4*A Right*) but not in an exposed wild-type dog (Fig. 4*B*). Of note, the superior lesion was larger (3.5-mm diameter) than the inferior lesion (2 mm) although the focal light exposure in both locations was the same size and intensity. Both lesions were smaller at 4 wk than the appearance of the retinal alterations at 24 h (≈4-mm diameter, Fig. 2*A*).

Histopathology performed at 4 wks showed a transition from normal retina outside the focal exposure (Fig. 4 *C*) to a boundary region where the retinal architecture abruptly changed from normal to diseased (Fig. 4 *D*). In this area, the photoreceptors decreased in number and length, and their nuclei became dispersed. Near the center of the area of light exposure, there was severe retinal degeneration (11), but the lesions were not identical in tapetal and nontapetal regions. In the tapetal region (Fig. 4*E*), there was near complete loss of RPE and photoreceptors. A single, incomplete row of photoreceptor nuclei remained, and these had the cytologic features of cones. In contrast, the nontapetal region had an intact RPE cell layer, but the density of pigmentation varied from moderate to absent, and some cells had migrated into the subretinal space (Fig. 7, which is published as supporting information on the PNAS web site). Rudimentary photoreceptor IS remained, and the

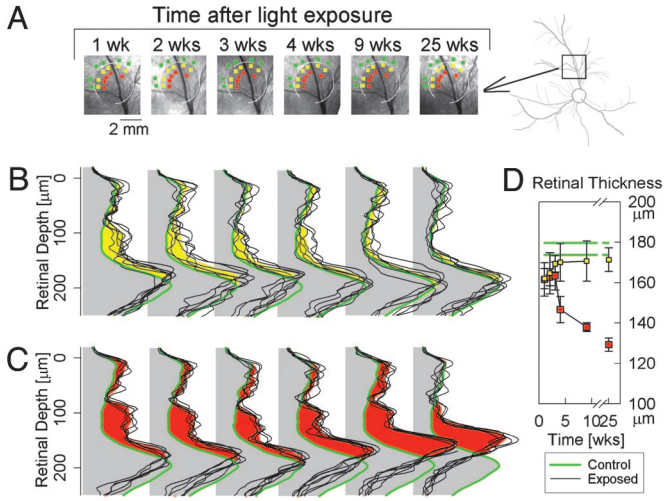

Fig. 5. Slow repair and slow degeneration with lower light exposures. (*A*) *En face* infrared imaging in the superior retina shows the progressive reduction of the extent and fading of a visible circular lesion over 25 wk. White arcs demarcate the extent of the lesion at 1 wk. Data from locations near the exposure boundary (yellow squares), more central to the lesion (red squares), and peripheral to exposure boundary (green squares) are shown in detail (*B* and *C*). (*A Far Right*) Retinal vessel map with black square showing location of *en face* images. (*B* and *C*) LRPs from individual locations (thin black traces) near the inside boundary (*B*) or more central to the lesion (*C*) and average control (thick green line) locations near the outside boundary of the lesion at various times after a focal exposure of 6 mJ·cm^{-2}. The difference of mean scattering between inside versus outside the boundary is shown as yellow (*B*) or red (*C*). (*D*) Retinal thickness derived from the cross-sectional scans in *B* and *C* plotted as a function of time after the light exposure. Data points are mean ± 1 SD. Green lines show the control thickness (mean ± 1 SD) derived from unexposed green loci.

ONL had an incomplete row of cone nuclei. In both areas, the inner retinal layers were preserved.

Repair or Degeneration Occurs Slowly After 10-Fold Less Light Exposure. Having found extreme vulnerability of the *RHO* mutant retina to clinical levels of light, we reduced the retinal irradiance of the focal light exposure by 10-fold (6 mJ·cm^{-2}) and studied the spatial–temporal consequences. By *en face* imaging, there were no detectable abnormalities over the 6-month observation period in the inferior retina. In the superior retinal locus, however, there was a dark lesion visible at early times after the light exposure, and the extent of this lesion became progressively smaller over the next 6 months (Fig. 5*A*). Cross-sectional imaging analyses with LRPs were performed at locations near the exposure boundary (yellow squares), more central to it (red squares), and more peripheral to it (green squares) in nonexposed retina (Fig. 5*A*).

At 1 wk after light exposure, the pattern of intraretinal light scatter was similar at the border and central regions; there was an abnormal increase in backscatter encompassing the length of the photoreceptor layer (Fig. 5 *B* and *C*). Peak reflection had moved vitreally, similar to that seen at early times after the higher light exposure (Fig. 2*D*). Between 2 and 25 wk after exposure, the intraretinal scatter of the border region became progressively less abnormal, and peak reflection moved sclerad toward the control depth. By 25 wk, there were no differences between LRPs of the border region and more peripheral nonexposed retina (Fig. 5*B*).

At retinal locations toward the center of the exposed region, there was a 3-wk period during which there were no detectable changes to the abnormal intraretinal light scatter or retinal thickness (Fig. 5*C*, left three traces). Between 4 and 25 wk, however, there was progressive thinning of the retina (Fig. 5*C*, right three traces). The thickness at 25 wk approximated that observed at 4 wk after the more intense focal light exposure (Fig. 4*A*). Serial retinal thickness measurements illustrated the delayed onset and then progressive retinal degeneration after light exposure in the *RHO* mutant dog (Fig. 5*D*).

Discussion

Long-term survival of postmitotic neurons under acute or chronic stress depends on the balance between pro- and antiapoptotic signaling, as well as success or failure of cellular repair-compensation mechanisms (1, 25, 26). To study these mechanisms *in vivo*, we titrated a transient increase in neuronal stress by focal light exposure of a region of retina in the *RHO* mutant dog, a recently identified naturally occurring large animal model of the most common form of human retinal degeneration (11). Early alterations in retinal tissue were detectable *in vivo* in minutes after light exposure and were followed sequentially for up to 6 months. There was a dose-response relationship between light exposure and long-term outcomes of these early alterations. Highest doses of light caused rapid loss of neurons, reaching complete degeneration of photoreceptors in <4 wk. The lowest doses of light exposure revealed mechanisms acting over a time scale of weeks to months that repaired the abnormal alterations resulting from neuronal stress. Repair of retinal injury has not been previously reported in chronic and slowly progressive inherited retinal degenerations. Taken together with previously demonstrated strong similarities in pathophysiological phenotype between the naturally occurring canine disease and a major subset of human autosomal dominant RP (11, 12), current results imply that continuous repair of neuronal stress caused by light may contribute to the natural history of disease progression observed in patients. Further, the experimental paradigms defined in the *RHO* mutant dog may provide a convenient model to parse the underlying molecular mechanisms of neuronal repair.

Earliest retinal alterations caused by neuronal stress consisted of increased backscattering originating from the depth of the full length of photoreceptors; this abnormality was not isotropic and followed a distal to proximal pattern. Distal changes near the photoreceptor OS–RPE interface developed quickly and resulted in ≈10-fold increase of light backscatter by 1 h as compared with neighboring unexposed retina; by 3.5 h, the distal changes were not observable (Fig. 1). Loss of the highly organized membrane structure of the OS disks may be the cause of this increased light scattering (18, 27–29). The shedding of OS disks and their engulfment by the RPE observed at 2 h in a *RHO* mutant dog (Fig. 3) would explain the disappearance of this alteration.

Increase of light scatter originating from more proximal retinal depths of OPL through IS/OS boundary developed more slowly after light exposure and resulted in ≈8-fold increases compared with control by 24 h (Fig. 2). There are many potential causes of intraretinal scatter, such as glial or neuronal swelling, plasma membrane blebbing, nuclear pyknosis, and extracellular fluid accumulation; morphological evidence for some of these alterations was present at 24 h. A plausible and mechanistically interesting source of the intraretinal scatter (evident in minutes) would be structural abnormalities in mitochondria. Mitochondria are centrally involved in the initiation and execution of apoptosis upon integrating cellular stress signals (30, 31) and are also believed to have an optical role in the retina. Their fission or swelling (18) could result in changes in intracellular refractive index gradients (20, 32) and cause increased tissue backscatter.

Very slow dynamics of progressive retinal thinning observed after incrementally higher light exposures in the *RHO* mutant dogs were very different from the synchronized and fast apoptosis observed over a period of hours to days in previous experimental paradigms involving photochemical damage (33). Especially unexpected was a static period of 3 wk preceding the 5-month period of progressive retinal degeneration. The static period could represent the continuum between failure of repair mechanisms and the slow

development of adaptive/compensatory changes in photoreceptors, which would increase the risk of apoptosis (15, 34). Ensuing months would correspond to stochastic loss of previously light-exposed neurons. Alternative explanations for the delayed and slow degeneration include secondary effects such as release of toxic factors, withdrawal of survival factors, or damage to the RPE or glial cells, all of which could have been caused by acute death of a small subset of photoreceptors shortly after the light exposure (35). Such an argument, however, would have to predict centrifugal expansion of focal lesions over time, which was not observed in the current work.

We propose three general coping responses to light in canine *RHO* mutant photoreceptors and speculate about relationships to human *RHO* disease (Fig. 8, which is published as supporting information on the PNAS web site). Relatively low doses of light can lead to photoreceptor OS shedding and abnormal backscatter throughout the cell. Repair mechanisms are successful, and the risk of apoptosis becomes no different from that due to the mutant steady state (15). Moderate doses of light cause a partially dysfunctional (compensated) photoreceptor with a heightened risk of apoptosis, leading to slow degeneration. With higher doses of light, repair and compensation mechanisms are overwhelmed, and there is a large increase in risk of apoptosis and faster rate of degeneration. Two well-known features of the human phenotype may be interpreted in the context of these canine experiments. First, patients with *RHO* mutations (Class B1, ref. 12) have visual loss that is not uniform across the retina although all retinal rod photoreceptors should harbor mutant rhodopsin (36). There is increased risk of apoptosis in the inferior retina (superior visual field) where environmental light dose is expected to be higher (e.g., refs. 10 and 12 and Fig. 8*B*). Rather than a concept of disease spread by contiguous extension from initial foci of damage, we suggest that visual losses in *RHO* mutations occur in relationship to light dosage. Retinal areas with greater light exposure have faster degeneration than areas receiving lower doses. The latter may have balanced pro- and antiapoptotic signaling but degenerate later from failed cellular repair-compensation mechanisms. Second, slowed kinetics of rod dark adaptation after light exposure is a phenotypic marker of this subset of human *RHO* mutations (ref. 12 and Fig. 8*C*). The late and slow phase of recovery, which can extend for days, has had an uncertain basis. A hypothesis that this may represent repair after light-induced photoreceptor OS shedding (37) gains support from the repair process found in light-exposed canine *RHO* mutant retina.

Our work in a large-animal model of the *RHO* mutant form of RP, taken together with transgenic rodent studies (8, 9), leads to clinical recommendations that, of course, are tempered by species differences as well as the wide spectrum of human *RHO* mutations. Immediately, it would be judicious to modify clinical examination of patients with *RHO* mutations. Retinal photography should not be standard in these patients, retinal examinations should be of short duration by using the least light possible, and light exposure during ocular surgery should be reduced. Longer term recommendations relate to the design of preclinical and clinical trials for *RHO* mutations. Whether gene-specific or gene-independent, proposed interventions involving intraocular surgery and traditional bright light visualization techniques need to be concerned about the complicating effects of light exposure on outcome. Outcome measures, such as photographic montages and prolonged light-adapted cone flicker ERGs (untested in the current experiments), may be ill-advised. In summary, the current experiments examining a gene–environmental interaction in the *RHO* mutant dog not only provide a useful *in vivo* assay to study underlying mechanisms of retinal repair and degeneration but also represent preclinical data arguing for a carefully designed gene-specific clinical trial of light reduction in humans with adRP from *RHO* mutations.

We thank S. B. Schwartz, M. J. Pianta, A. J. Roman, T. M. Redmond, R. W. Knighton, A. Nickle, M. Swider, W. C. Nyberg, M. Roman, A. Y. Cheung, A. Pantelyat, E. E. Smilko, E. A. M. Windsor, V. Bhuva, P. Schied, J. Jordan, and P. Hammond for critical help. This work was supported by grants from the National Institutes of Health, the Foundation Fighting Blindness, the Macula Vision Research Foundation, the F. M. Kirby Foundation, the Macular Disease Foundation, Research to Prevent Blindness, the Mackall Foundation, the National Organization of the Blind from Spain (ONCE) International Prize, and the Van Sloun Fund.

1. Benn, S. C. & Woolf, C. J. (2004) *Nat. Rev. Neurosci.* **5,** 686–700.
2. Pacione, L. R., Szego, M. J., Ikeda, S., Nishina, P. M. & McInnes, R. R. (2003) *Annu. Rev. Neurosci.* **26,** 657–700.
3. Organisciak, D. T. & Winkler, B. S. (1994) *Prog. Ret. Eye Res.* **13,** 1–29.
4. Jacobson S. G. & McInnes, R. R. (2002) *Nat. Genet.* **32,** 215–216.
5. Wenzel, A., Grimm, C., Samardzija, M. & Reme, C. E. (2005) *Prog. Ret. Eye Res.* **24,** 275–306.
6. Dryja, T. P., McGee, T. L., Hahn, L. B., Cowley, G. S., Olsson, J. E., Reichel, E., Sandberg, M. A. & Berson, E. L. (1990) *N. Engl. J. Med.* **323,** 1302–1307.
7. Seyedahmadi, B. J., Rivolta, C., Keene, J. A., Berson, E. L. & Dryja, T. P. (2004) *Exp. Eye Res.* **79,** 167–173.
8. Naash, M. L., Peachey, N. S., Li, Z. Y., Gryczan, C. C., Goto, Y., Blanks, J., Milam, A. H. & Ripps, H. (1996) *Invest. Ophthalmol. Vis. Sci.* **37,** 775–782.
9. Organisciak, D. T., Darrow, R. M., Barsalou, L., Kutty, R. K. & Wiggert, B. (2003) *Invest. Ophthalmol. Vis. Sci.* **44,** 486–492.
10. Heckenlively, J. R., Rodriguez, J. A. & Daiger, S. P. (1991) *Arch. Ophthalmol.* **109,** 84–91.
11. Kijas, J. W., Cideciyan, A. V., Aleman, T. S., Pianta, M. J., Pearce-Kelling, S. E., Miller, B. J., Jacobson, S. G., Aguirre, G. D. & Acland, G. M. (2002) *Proc. Natl. Acad. Sci. USA* **99,** 6328–6333.
12. Cideciyan, A. V., Hood, D. C., Huang, Y., Banin, E., Li, Z.-Y., Stone, E. M., Milam, A. H. & Jacobson, S. G. (1998) *Proc. Natl. Acad. Sci. USA* **95,** 7103–7108.
13. Berson, E. L., Sandberg, M. A., Rosner, B., Birch, D. G. & Hanson, A. H. (1985) *Am. J. Ophthalmol.* **99,** 240–251.
14. Hoffman, D. R., Locke, K. G., Wheaton, D. H., Fish, G. E., Spencer, R. & Birch, D. G. (2004) *Am. J. Ophthalmol.* **137,** 704–718.
15. Clarke, G., Collins, R. A., Leavitt, B. R., Andrews, D. F., Hayden, M. R., Lumsden, C. J. & McInnes, R. R. (2000) *Nature* **406,** 195–199.
16. Lawwill, T., Crockett, S. & Currier, G. (1977) *Doc. Ophthalmol.* **44,** 379–402.
17. Gorgels, T. G. & van Norren, D. (1995) *Invest. Ophthalmol. Vis. Sci.* **36,** 851–863.
18. Busch, E. M., Gorgels, T. G. & van Norren, D. (1999) *Vision Res.* **39,** 1233–1247.
19. Schuman, J. S., Puliafito, C. A. & Fujimoto, J. G. (2004) *Optical Coherence Tomography of Ocular Diseases* (Slack, Thorofare, NJ), 2nd Ed.
20. Huang, Y., Cideciyan, A. V., Papastergiou, G. I., Banin, E., Semple-Rowland, S. L., Milam, A. H. & Jacobson, S. G. (1998) *Invest. Ophthalmol. Vis. Sci.* **39,** 2405–2416.
21. Huang, Y., Cideciyan, A. V., Aleman, T. S., Banin, E., Huang, J., Syed, N. A., Petters, R. M., Wong, F., Milam, A. H. & Jacobson, S. G. (2000) *Exp. Eye Res.* **70,** 247–251.
22. Jacobson, S. G., Cideciyan, A. V., Aleman, T. S., Pianta, M. J., Sumaroka, A., Schwartz, S. B., Smilko, E. E., Milam, A. H., Sheffield, V. C. & Stone, E. M. (2003) *Hum. Mol. Genet.* **12,** 1073–1078.
23. Adamus, G., Zam, Z. S., Arendt, A., Palczewski, K., McDowell, J. H. & Hargrave, P. A. (1991) *Vision Res.* **31,** 17–31.
24. Gorski, K., Carneiro, M. & Schibler, U. (1986) *Cell* **47,** 767–776.
25. Stone, J., Maslim, J., Valter-Kocsi, K., Mervin, K., Bowers, F., Chu, Y., Barnett, N., Provis, J., Lewis, G., Fisher, S. K., *et al.* (1999) *Prog. Retin. Eye Res.* **18,** 689–735.
26. Haynes, C. M., Titus, E. A. & Cooper, A. A. (2004) *Mol. Cell.* **15,** 767–776.
27. Kuwabara, T. (1970) *Am. J. Ophthalmol.* **70,** 187–198.
28. Moriya, M., Baker, B. N. & Williams, T. P. (1986) *Cell Tissue Res.* **246,** 607–621.
29. Wenzel, A., Grimm, C., Marti, A., Kueng-Hitz, N., Hafezi, F., Niemeyer, G. & Reme, C. E. (2000) *J. Neurosci.* **20,** 81–88.
30. Shaulian, E. & Karin, M. (2002) *Nat. Cell Biol.* **4,** E131–E136.
31. Hao, W., Wenzel, A., Obin, M. S., Chen, C. K., Brill, E., Krasnoperova, N. V., Eversole-Cire, P., Kleyner, Y., Taylor, A., Simon, M. I., *et al.* (2002) *Nat. Genet.* **32,** 254–260.
32. Hoang, Q. V., Linsenmeier, R. A., Chung, C. K. & Curcio, C. A. (2002) *Vis. Neurosci.* **19,** 395–407.
33. Hafezi, F., Marti, A., Munz, K. & Reme, C. E. (1997) *Exp. Eye Res.* **64,** 963–970.
34. Zhu, X., Raina, A. K., Perry, G. & Smith, M. A. (2004) *Lancet Neurol.* **3,** 219–226.
35. Leveillard, T., Mohand-Said, S., Lorentz, O., Hicks, D., Fintz, A. C., Clerin, E., Simonutti, M., Forster, V., Cavusoglu, N., Chalmel, F., *et al.* (2004) *Nat. Genet.* **36,** 755–759.
36. Papermaster, D. S. & Windle, J. (1995) *Invest Ophthalmol. Vis. Sci.* **36,** 977–983.
37. Moore, A. T., Fitzke, F. W., Kemp, C. M., Arden, G. B., Keen, T. J., Inglehearn, C. F., Bhattacharya, S. S. & Bird, A. C. (1992) *Br. J. Ophthalmol.* **76,** 465–469.

Supporting Information For
Cideciyan et al. In vivo dynamics of retinal injury and repair in the rhodopsin mutant dog model of human retinitis pigmentosa. Proc Natl Acad Sci 102:5233-5238, 2005.

Supporting Figure 6. Properties of the light used to perform the focal exposures under Maxwellian view and simultaneous infrared visualization (CPP-1, Cannon, Lake Success, NY) in mutant and wildtype dogs. *(A)* Spectral distribution (USB 2000, Ocean Optics, Dunedin, FL) of the focal exposure light (tungsten-halogen bulb) measured at the cornea peaked near 585 nm due to filtering through multiple glass lenses (causing absorption of shorter wavelengths) and a set of two consecutive infrared-blocking filters (causing absorption of longer wavelengths). *(B)* Spatial distribution of the circular focal light along the horizontal meridian (squares). The ideal light distribution (lines) corresponds to a central ~3 mm diameter uniform region surrounded by ~0.5 mm wide annulus showing linear light fall-off due to optical vignetting.

Supporting Figure 7. Histological changes in the inferior retina 4 wks after focal exposure in the same *RHO* mutant dog as shown in Fig. 4A (see Fig.4 C – E for the histological changes in the superior retina). Regions shown are outside, inside and at the border between light-exposed and non-exposed regions. (*A*) Outside the lesion, the retina is normal. (*B*) There are abrupt changes at the border with loss of outer retinal tissue. RPE artefactually detached. (*C*) Inside the light-exposed area, an incomplete row of cone photoreceptor nuclei remain; RPE are detached from the monolayer and have migrated into the subretinal space.

Supporting Figure 8. Hypothesized consequences of light exposure on *RHO* mutant photoreceptors in canine and human retinas. *(A)* Schematic representation of three major coping responses observed in canine *RHO* mutant retinas. Relatively low doses of light result in OS shedding and abnormal backscatter throughout the photoreceptor that can be successfully repaired over extended periods of time. Moderate doses of light cause a partially dysfunctional (compensated) photoreceptor with a heightened risk of apoptosis leading to slow degeneration. With higher doses of light, repair and compensation mechanisms are overwhelmed and there is large increase in risk of apoptosis and a fast degeneration. *(B)* Slow progression of visual field loss over 10-15 years in representative human *RHO* mutations (Class B1; ref. 12) is consistent with a higher risk of apoptosis in the inferior retina (superior visual field), which is expected to receive higher environmental light exposure. *(C)* Kinetics of psychophysical thresholds in the dark following a controlled light exposure in representative human *RHO* mutations has a fast initial phase, corresponding to a physiological recovery, and a slow final phase, corresponding to neuronal repair.

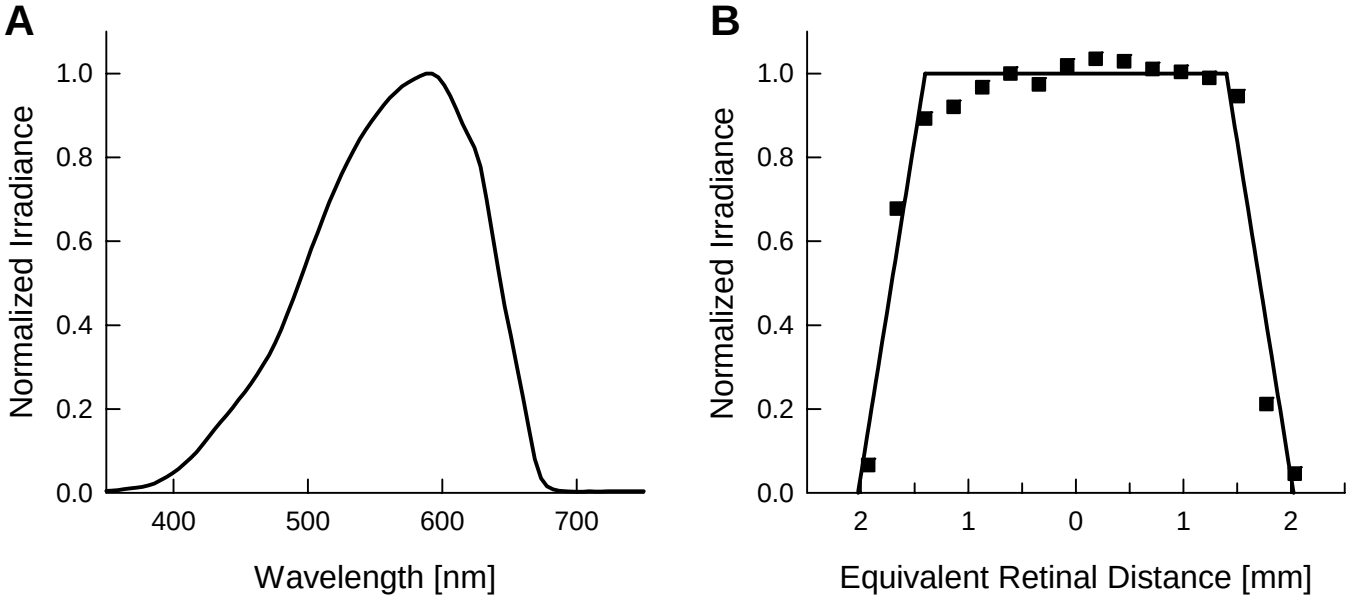
A
Normalized Irradiance
1.0
0.8
0.6
0.4
0.2
0.0
400
500
600
700
Wavelength [nm]
B
Normalized Irradiance
1.0
0.8
0.6
0.4
0.2
0.0
2
1
0
1
2
Equivalent Retinal Distance [mm]

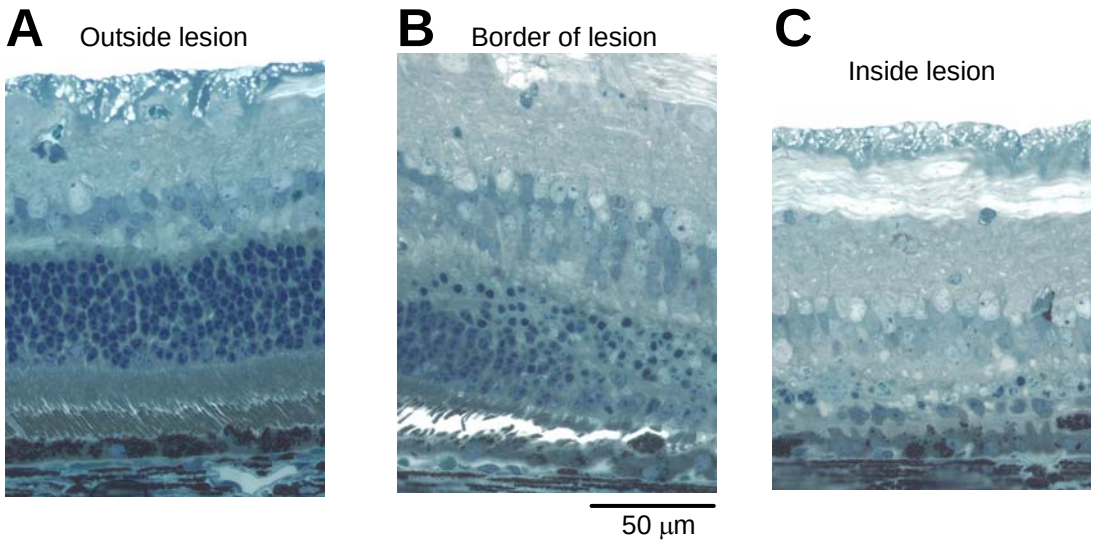
A
Outside lesion
B
Border of lesion
C
Inside lesion
50 μm

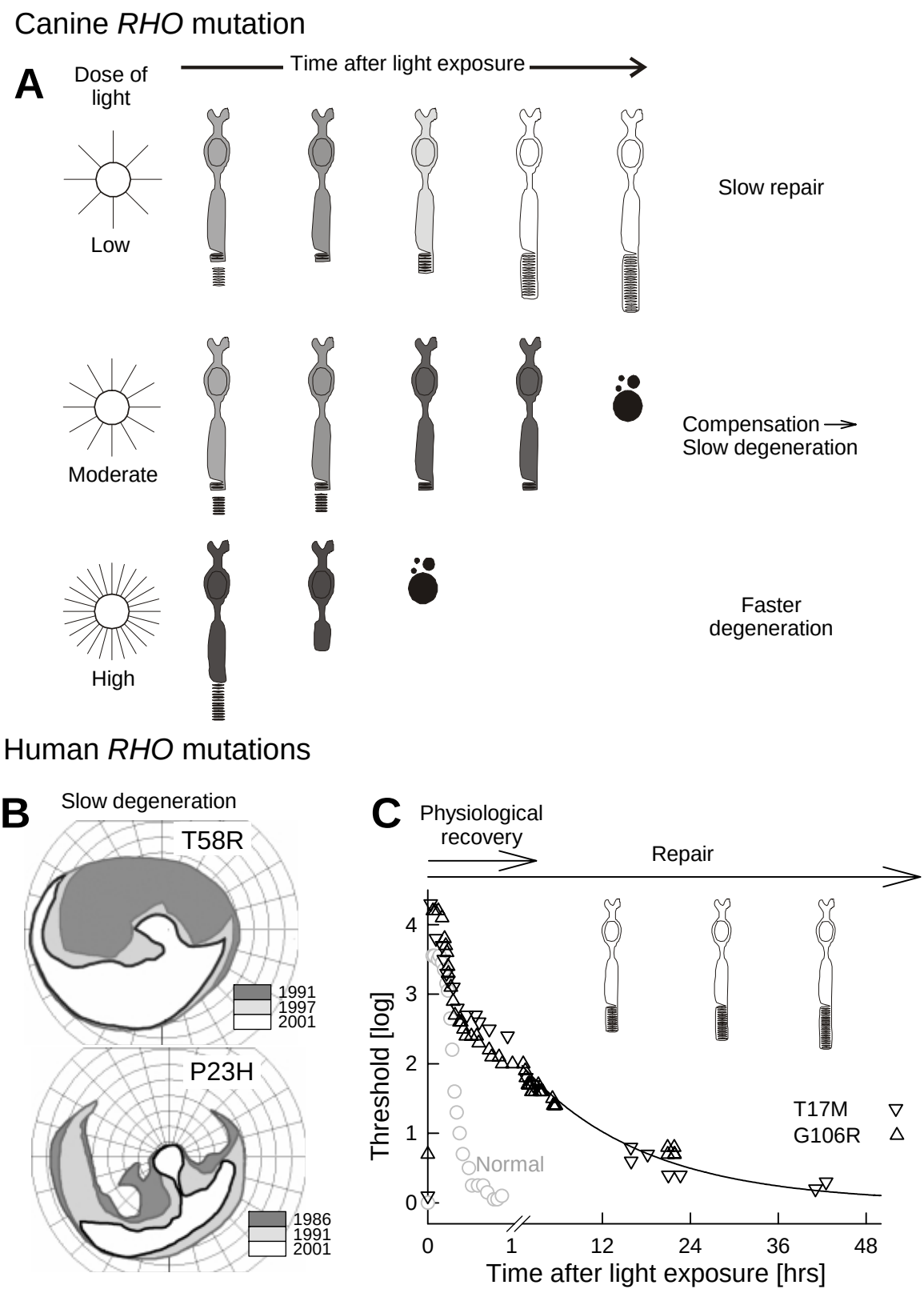
Canine *RHO* mutation
A
Dose of light
Time after light exposure
Low
Slow repair
Moderate
Compensation
Slow degeneration
High
Faster degeneration
Human *RHO* mutations
B
Slow degeneration
T58R
1991
1997
2001
P23H
1986
1991
2001
C
Physiological recovery
Repair
Threshold [log]
0
1
2
3
4
T17M
G106R
Normal
0
1
12
24
36
48
Time after light exposure [hrs]